Icarus 309 (2018) 61–68

Contents lists available at ScienceDirect

Icarus

journal homepage: www.elsevier.com/locate/icarus

Investigation of the depth and diameter relationship of subkilometer-diameter lunar craters

Shujuan Sun[a], Zongyu Yue[b,*], Kaichang Di[b]

[a] The Third Remote Sensing Geoinformatics Institute of National Administration of Surveying, Mapping and Geoinformation, Chengdu 610100, China
[b] State Key Laboratory of Remote Sensing Science, Institute of Remote Sensing and Digital Earth, Chinese Academy of Sciences, Beijing 100101, China

ARTICLE INFO

Article history:
Received 22 May 2017
Revised 4 January 2018
Accepted 27 February 2018
Available online 6 March 2018

Keywords:
Depth
Diameter
Small crater
Lunar

ABSTRACT

The depth and diameter relationship is one of the most important characteristics of craters; however, previous studies have focused mostly on large-diameter craters because of the limitations of image resolution. Recently, very high resolution images have been obtained that make it possible to expand this field of study to craters with diameters of < 1 km. Using images with resolution of up to 0.5 m, acquired by the Lunar Reconnaissance Orbiter, we investigated the depth and diameter relationship of fresh craters with subkilometer diameters. We selected craters from lunar maria and highlands, and we made precise measurements of their diameters and depths. The results show that the *d*/*D* ratio of small craters in the lunar maria and highlands, which varies from ~0.2 to ~0.1, is generally shallower than that of larger craters. We propose that the reason for the difference is because of the low strength of the lunar surface material. The fitted power law parameters of lunar mare and highland craters were found to be different, and that might be explained by terrain-related differences.

1. Introduction

The surfaces of terrestrial planets are covered by myriad large and small craters. The study of the morphological characteristics of craters is important for furthering our understanding of both the impact cratering process and target properties. The morphology of craters on terrestrial planets becomes much more complex with increasing diameter, and the relationship between crater diameter and depth has always been a focus in related studies. Among the initial data used for investigating crater depth and diameter are the Ranger Lunar Charts (RLC) published by the Aeronautical Chart and Information Center, which contain depth and diameter of craters using data derived from the Ranger missions. Baldwin (1963) presented a polynomial equation relating logarithmic rim-to-rim diameter (D) and rim-to-bottom depth (d), and revised the equation to be $D = 0.0256d^2 + d + 0.6300$ using 130 craters from RLC 1-5 data with $D = 0.008–42.0$ km (Baldwin, 1965). Using the same data source, Markov (1967) proposed that the logarithmic diameter-vs-depth relationship is nearly linear and may be represented by equation $D = 1.0662d + 0.6200$. Bouška (1968) studied 644 craters from RLC 7-12 (Ranger VIII) and RLC 14-17 (Ranger IX) photographs, including both primary and secondary craters. Bouška (1968) fitted the logarithmic diameters and depths with both polynomial and linear equations using the least squares method, and the results showed that the logarithmic diameter–depth relationship was practically linear for small craters. Pike (1974) proposed that Apollo photogrammetry data could yield more accurate measurements than did the shadow technique, and after investigating 204 fresh lunar craters 60 m to 275 km across, he found the depth/diameter distribution inflected at a crater diameter of 10–15 km, and for craters smaller than about 15 km across the depth/diameter distribution could be described by the equation $d = 0.196D^{1.010}$. By investigating apparent depth/apparent diameter relation for lunar craters, Pike (1977) drew similar conclusions and put forward that craters less than 900 m in apparent diameter (equivalent to a rim-crest diameter of 1084 m) may be subject to laws different from those of larger craters. It is necessary to point out that in early studies of the crater depth and diameter relationship, the depth-to-diameter (d/D) ratio has long been used as a key parameter in the description of crater morphology, and the d/D ratio is ~0.2 for primary simple craters on terrestrial planets, though different research works have derived values as low as ~0.15 and as high as ~0.22 (e.g., Pike, 1974, 1977, 1980; Wood and Anderson, 1978; Cintala and Mouginis-Mark, 1980; Stopar et al., 2017).

Recently, several space missions have acquired large amounts of high-resolution data, such as the Lunar Reconnaissance Orbiter (LRO) (Robinson et al., 2010), SELENE (Kato et al., 2010) and Chang' E 2 orbiter (Zhao et al., 2011) to the Moon, the Mars Orbiter Laser

* Corresponding author.
E-mail address: yuezy@radi.ac.cn (Z. Yue).

https://doi.org/10.1016/j.icarus.2018.02.031
0019-1035/

Altimeter (MOLA) on Mars Global Surveyor (Albee et al., 1998), the High Resolution Imaging Science Experiment (HiRISE) on the Mars Reconnaissance Orbiter (MRO) (Zurek and Smrekar, 2007) and the High Resolution Stereo Camera (HRSC) on Mars Express (Jaumann et al., 2007) to Mars. Salamuniccar et al. (2012) improved crater detection algorithms (CDAs) and identified many more lunar and martian craters using recent data (i.e., LRO Lunar Orbiter Laser Altimeter (LOLA), SELENE Laser Altimeter (LALT) for the Moon and MGS Mars Orbiter Laser Altimeter (MOLA) for Mars), resulting in the LU60645GT (up to $\sim D \geq 8$ km) and MA132843GT (up to $\sim D \geq 2$ km) catalogues of lunar and martian craters. However, Mouginis-Mark et al. (2017) reviewed the methods and datasets used to determine crater depth and diameter of martian craters, and proved that stereo photogrammetry was an intrinsically more accurate method for measuring depth and diameter of craters on Mars when applied to high-resolution image pairs (such as Context Camera and HiRISE). The advent of high-resolution data not only make it possible to study crater morphology in much more detail and greater accuracy, but also expand this field to smaller craters ($D < 1$ km).

There are already some studies on small crater morphology using recent high-resolution data. Mahanti et al. (2012) investigated the depth-to-diameter ratio of 540 lunar highland small craters (<150 m diameter) using LRO Narrow Angle Camera (NAC) and found a median value of ~0.13, and they proposed that the depth and diameter data could be better represented by a straight line rather than a power law relation. Mahanti et al. (2014) sampled small lunar craters globally from LRO NAC based Digital Elevation Models (DEMs) and obtained a median d/D of 0.13. Daubar et al. (2014) produced statistics on craters with diameters of 17–918 m in two regions of the lunar surface, for which an average d/D ratio of ~0.10 was derived. Daubar et al. (2014) also performed a similar study of martian fresh craters (formed in the last ~20 years), for which an average d/D ratio of 0.23 was derived. By examining a global population of small (25 m ≤ 5 km) and well-preserved simple impact craters using HiRISE stereo-derived elevation models, Watters et al. (2015) found that scaling laws from prior studies of large simple craters generally overestimate the depth and volume at small diameters, and get $d = 0.223D^{1.012}$ (d and D in kilometers). Stopar et al. (2017) found that the d/D ratios of small fresh lunar craters ($D < 400$ m) range from 0.11 to 0.17.

In this research, we used recently acquired LRO NAC data to perform a comprehensive study of the depth and diameter relationship of small best preserved craters in both lunar maria and highland regions, to analyze the depth and diameter relationship and characterize the terrain dependence of the shapes of best preserved craters. Furthermore, we performed a detailed comparison with related results from studies of other small lunar craters. This work could assist the study of the material properties of the lunar shallow surface because the morphologies of well-preserved simple craters are dominated by the target properties (Melosh, 1989). In this research, well-preserved craters were selected, and others excluded or filtered out, in order to minimize the effects of post-impact modification processes significantly affecting the craters' depths. While this process is somewhat subjective and the possibility of post-impact modification processes affecting these craters remains, there are no alternatives available.

2. Data

Lunar fresh small craters were selected from high-resolution, public LRO NAC DEMs. The LRO was launched on June 18, 2009 to facilitate mapping of the lunar surface at enhanced spatial scales (Vondrak et al., 2010). The LROC onboard the LRO includes a Wide Angle Camera (WAC) and two NACs. The former is a push-frame camera with resolutions of 75 and 384 m (at an altitude of 50 km) in the visible and ultraviolet bands, respectively, while the latter are monochrome narrow-angle line scan imagers with full resolution of 0.5 m (at an altitude of 50 km) (Robinson et al., 2010).

The LROC team (NASA/GSFC/Arizona State University) has published more than 380 LRO NAC DEMs, which can be downloaded from the LROC homepage (http://lroc.sese.asu.edu/). This study selected 14 lunar experimental regions, as shown in Fig. 1, comprising six maria regions (red dots) and eight highland regions (green dots). All these regions are covered by publically available NAC DEMs with pixel scale of 2.0 m. The six maria regions comprise the Apollo 11, 12, 14, 15, and 17 landing sites and another region located near the Apollo 14 landing site. The eight highland regions comprise the Apollo 16 landing site and seven other highland regions. The experimental regions are distributed widely over the lunar surface and sample a variety of terrains to ensure the derived statistics are representative.

Here, NAC mapping products, including DEMs and orthophotos from the DEMs, were used for identifying fresh small craters and for measuring their depths and diameters. Table 1 lists the data used in this study. For each experimental region, the data product with a letter 'E' in the file name represents a DEM file, while the data product with a letter 'M' in the file name represents an orthophoto of the same area. The orthophotos were used to select the craters, and the DEM data were used for the actual measurements. Most of the DEMs and corresponding orthophotos were co-registered, except for the data around Apollo 12 landing site. There was an offset between the DEM and orthophoto at the Apollo 12 landing site; thus, the orthophoto was first co-registered to the DEM before selecting the craters. The precision quoted for each DEM data product listed in Table 1 is from the reported precision errors from SOCET SET in the readme files associated with the DEM and orthophoto products (e.g., the precision error of Apollo 11 DEM can be found at http://lroc.sese.asu.edu/data/LRO-L-LROC-5-RDR-V1.0/LROLRC_2001/EXTRAS/BROWSE/NAC_DTM/APOLLO11/NAC_DTM_APOLLO11_README.TXT).

3. Method

3.1. Selection of fresh craters

Only fresh craters were selected for the measurements of depth and diameter. In earlier studies, fresh craters were identified by crisp rims and other interior morphological features, continuous ejecta fresh in appearance, and/or rays around the craters (e.g., Malin and Dzurisin, 1977; Pike, 1980). These criteria are also appropriate for this study; morphologically fresh craters that have no obvious degradation were selected for the statistical analysis. To ensure that craters could be identified clearly, the diameter of a crater was required to be at least 10 pixels because many artifacts occur with craters < 10 pixels across (Robbins et al., 2014). Taking the pixel size of NAC DEM products into consideration, the minimum reliable diameter of craters was limited to 20 m. Fig. 2 shows four examples of lunar fresh small craters.

3.2. Measurement of depth and diameter

The definitions of crater diameter D and crater depth d in this study are adopted from Barnouin et al. (2012), in which D refers to the distance through the crater center between crater rims, and d refers to the distance between the deepest point and the average rim height (Fig. 3).

For the identified fresh small craters, the rim-to-rim diameter D was measured with the help of *CraterTools*, an ArcMap plug-in (Kneissl et al., 2011), which can fit a crater with a circle or ellipse independent of projection. The crater depth d was calculated in three steps. First, by overlapping the fitted circle/ellipse and corresponding DEM data, the height of each pixel on the circle could be

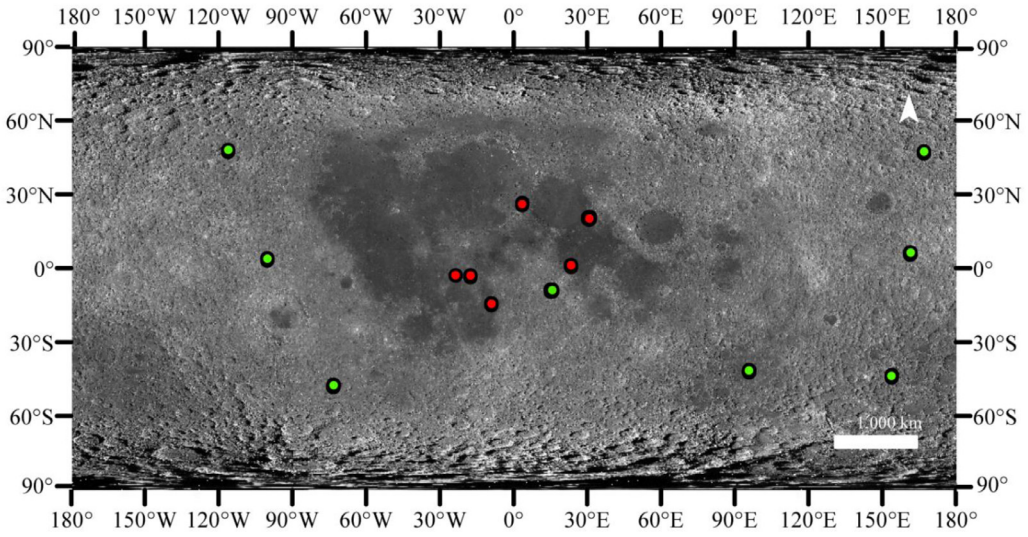

Fig. 1. Regions selected for experimental fresh lunar small craters. Mare regions are indicated by red dots and highland regions are indicated by green dots. The base map is an LROC WAC global mosaic product. (For interpretation of the references to color in this figure legend, the reader is referred to the web version of this article).

Table 1
Data products used in the statistical analysis of lunar fresh small craters.

Region	Center coordinates (N, E)	DEM and orthophotos	Pixel scale (m)	Precision of DEM (m)
Mare 1	(0.65, 23.51)	NAC_DTM_APOLLO11_E010N0230.IMG	2.0	0.77
		NAC_DTM_APOLLO11_M150361817_50CM.IMG	0.5	
Mare 2	(– 3.04, – 23.42)	NAC_DTM_APOLLO12_E030S3365.IMG	2.0	0.80
		NAC_DTM_APOLLO12_M120005333_50CM.IMG	0.5	
Mare 3	(– 3.66, – 17.48)	NAC_DTM_APOLLO14_E034S3425.IMG	2.0	0.76
		NAC_DTM_APOLLO14_M150633128_50CM.IMG	0.5	
Mare 4	(26.08, 3.65)	NAC_DTM_APOLLO15_E261N0036.IMG	2.0	1.06
		NAC_DTM_APOLLO15_M111571816_50CM.IMG	0.5	
Mare 5	(20.17, 30.77)	NAC_DTM_APOLLO17_E200N0310.IMG	2.0	1.06
		NAC_DTM_APOLLO17_MOSAIC_60CM.IMG	0.6	
Mare 6	(– 14.66, – 8.94)	NAC_DTM_LASELMASIF1_E147S3510.IMG	2.0	0.82
		NAC_DTM_LASELMASIF1_M152932948_50CM.TIF	0.5	
Highland 1	(– 43.90, 153.90)	NAC_DTM_WEIRDCRTR_E440S1538.IMG	2.0	1.87
		NAC_DTM_WEIRDCRTR_M187226851_70CM.TIF	0.7	
Highland 2	(– 8.99, 15.51)	NAC_DTM_APOLLO16_E90S0160.IMG	2.0	0.90
		NAC_DTM_APOLLO16_MOSAIC_50CM.IMG	0.5	
Highland 3	(– 41.84, 95.94)	NAC_DTM_JENNER_E419S0959.IMG	2.0	1.70
		NAC_DTM_JENNER_M1148861003_70CM.TIF	0.7	
Highland 4	(47.07, 166.93)	NAC_DTM_IMPACTMELT1_E470N1670.IMG	2.0	1.73
		NAC_DTM_IMPACTMELT1_M110498640_60CM.TIF	0.6	
Highland 5	(5.92, 161.42)	NAC_DTM_MNDLSHTMLS_E059N1614.IMG	2.0	2.00
		NAC_DTM_MNDLSHTMLS_M161245596_50CM.TIF	0.5	
Highland 6	(3.58, – 100.13)	NAC_DTM_NEARLENTS1_E030N2600.IMG	2.0	1.20
		NAC_DTM_NEARLENTS1_M151169370_70CM.TIF	0.7	
Highland 7	(47.58, – 116.11)	NAC_DTM_FRSHCRATER10_E480N2440.IMG	2.0	1.19
		NAC_DTM_FRSHCRATER10_M153639872_50CM.TIF	0.5	
Highland 8	(– 47.95, – 73.23)	NAC_DTM_ORIENTALE3_E480S2870.IMG	2.0	1.92
		NAC_DTM_ORIENTALE3_M186347549_60CM.TIF	0.6	

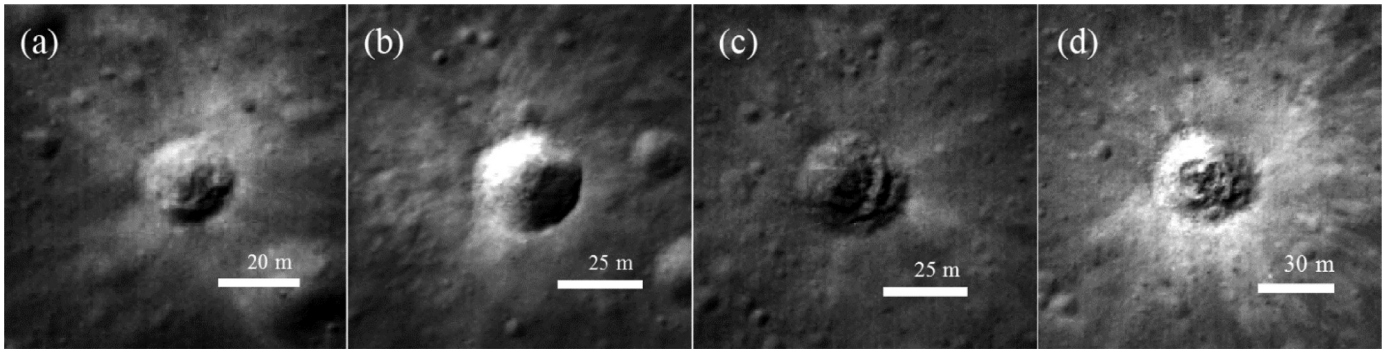

Fig. 2. Examples of lunar fresh small craters selected from the LRO NAC product NAC_DTM_APOLLO15_M111571816_50CM.IMG (north is up). (a) located at 26.28°N, 3.59°E, diameter: 21.49 m; (b) located at 25.74°N, 3.52°E, diameter: 30.3 m; (c) located at 26.31°N, 3.67°E, diameter: 32.21 m; and (d) located at 26.16°N, 3.62°E, diameter: 39.09 m.

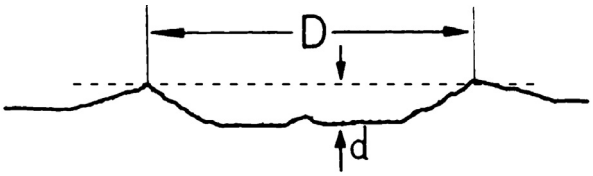

Fig. 3. Definitions of crater diameter D and depth d used in this study.

Table 2
Information of demo craters in Fig. 4.

Crater	Center coordinates (N, E)	d(m)	D(m)	d/D
a	(−44.13, 153.80)	5.03	38.24	0.13
b	(−44.25, 153.90)	1.97	20.06	0.10
c	(−44.15, 153.82)	1.50	24.81	0.06

obtained, and the average height was derived as the representative elevation of the crater rim. Second, all the pixels inside the circle were looped to determine the deepest point. Third, crater depth d was then calculated as the difference in elevation between the average and the deepest point within the crater.

For small craters with a diameter ~20 m, we produced hillshade maps from corresponding DEM products to help determine whether they could be considered as fresh craters. The hillshade maps were produced using ArcMap software, setting azimuth angle to be 315° and altitude angle to be 45°, respectively. Fig. 4 demonstrates how hillshade maps could be used to eliminate the shallowest craters, with Fig. 4(a)–(c) are three craters on NAC images and Fig. 4(d)–(f) are craters on corresponding hillshade maps. Information about these three craters is shown in Table 2. In Fig. 4(a)–(c), the three craters all look fresh and are selected for statistics. However, height variation can only be observed in (d), not in (e) and (f). According to Table 2 the craters in Fig. 4(b) and (c) are very shallow, indicating that the LRO NAC DEM products may not provide accurate depth of these two craters. If craters like Fig. 4(b) and (c) are included in statistics, the results would not be reliable. Therefore, such craters are removed in this research. If the height difference of a fresh-looking crater could be observed from the hillshade map, it was considered as a fresh crater (e.g., Fig. 4(a)); otherwise, it was excluded from further statistical analysis (e.g., Fig. 4(b) and (c)).

3.3. Uncertainties

The possible error sources of our method mainly consist of random error of crater diameter measurement and consequent error of crater depth. Repetitive experiments were conducted to assess the effect of these possible errors on final statistics.

Craters were divided into groups according to crater diameter, with the crater diameter of the first group between 20 and 30 m, the second group 30–40 m, …, 80–90 m (Considering that craters larger than 90 m were rare, crater diameter of the last group were limited to 80–90 m) to ensure the reliability of experiments. Two craters were randomly selected from each group, therefore 14 craters were selected altogether and the diameter of each crater were measured three times using *CraterTools* (Kneissl et al., 2011). Fig. 5 illustrated one of these craters, with each measurement indicated by different colors. The diameters of three measurements were 38.47 m (red circle), 38.67 m (black circle) and 38.78 m (blue circle), respectively, resulting in a mean diameter of 38.64 m and standard deviation of 0.13 m. The depth of these craters was also measured three times separately, leading to 5.62 m (red circle), 5.66 m (black circle) and 5.66 m (blue circle), respectively. Therefore, the mean depth of this crater was 5.65 m, with standard deviation of 0.02 m.

The results of repetitive experiments of all 14 craters are shown in Table 3, including the percentage error of standard deviation of

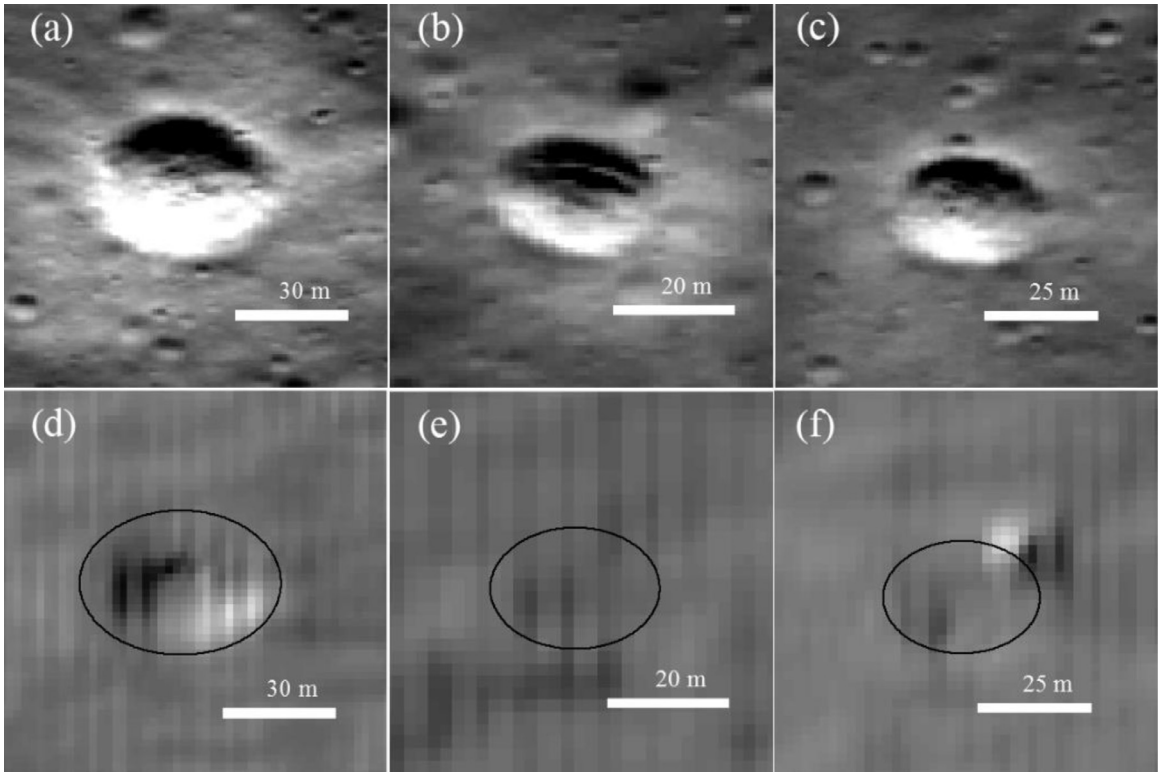

Fig. 4. Examples of lunar fresh small craters on LRO NAC product (NAC_DTM_WEIRDCRTR_M187226851_70CM.IMG) and corresponding hillshade map, north is up. (a)–(c) are craters on LRO NAC images, and (d)–(f) are the same craters on corresponding hillshade maps.

Table 3
Parameters of craters in repetitive experiments. D_STD and d_STD refer to standard deviation of diameter and depth, respectively.

Crater no.	Center coordinates (N, E)	Mean D (m)	D_STD (m)	Percentage error of D_STD (%)	Mean d (m)	d_STD (m)	Percentage error of d_STD (%)
1	(25.74, 3.51)	29.94	0.26	0.87	7.94	0.02	0.25
2	(25.77, 3.55)	25.55	0.18	0.70	7.90	0.07	0.89
3	(26.16, 3.62)	38.64	0.13	0.34	5.65	0.02	0.35
4	(26.48, 3.62)	37.68	0.26	0.69	3.44	0.02	0.58
5	(−9.37, 15.14)	61.16	0.51	0.83	9.37	0.01	0.11
6	(−9.28, 15.77)	45.82	0.55	1.20	8.00	0.06	0.75
7	(−9.29, 15.79)	43.66	0.22	0.50	7.52	0.01	0.13
8	(19.83, 30.71)	84.79	0.19	0.22	14.50	0.08	0.55
9	(20.17, 30.39)	54.58	0.47	0.86	10.33	0.14	1.36
10	(−9.05, 15.16)	60.96	0.59	0.97	11.38	0.02	0.18
11	(−3.09, −17.48)	75.14	0.60	0.80	13.94	0.07	0.50
12	(−3.67, −17.44)	54.73	0.52	0.95	8.55	0.01	0.12
13	(0.38, 23.42)	89.78	0.15	0.17	11.56	0.01	0.09
14	(−44.07, 153.99)	77.60	0.38	0.49	12.14	0.04	0.33

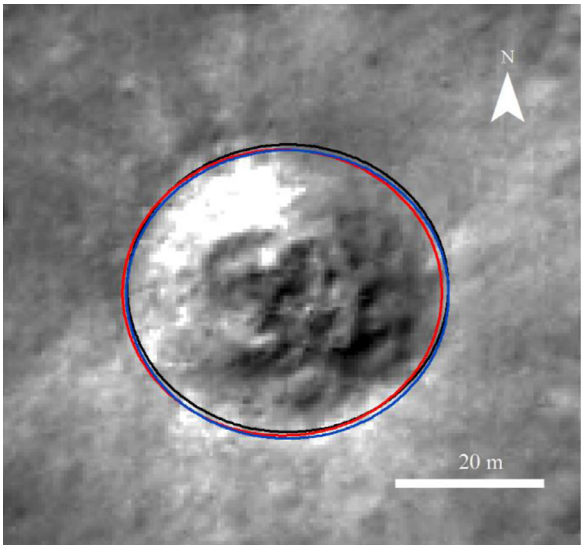

Fig. 5. An example crater (3.62°E, 26.16°N) of repetitive measurement. Three circles with different colors were all generated by CraterTools (Kneissl et al., 2011), and each was generated separately by selecting three different points on the crater rim. (For interpretation of the references to color in this figure legend, the reader is referred to the web version of this article).

diameter and depth. The maximum standard deviation of diameter among these craters is 0.60 m, compared with crater diameter of 75.14 m, the percentage error of diameter standard deviation of this crater is only 0.8%. However, the resulting standard deviation of depth of these craters is only 0.07 m, and the percentage error of depth standard deviation is 0.50%. The maximum standard deviation of depth among these craters is 0.14 m, and the percentage error of depth standard deviation of this crater is only 1.36%. The result indicates that the measurement of crater diameter and depth is reliable with small standard deviation, which gives an idea of variation between repetitive measurements.

4. Results

Table 4 shows the number of lunar fresh small craters selected in all the experimental regions. Initially, 891 craters were selected, but this number was reduced to 849 after filtering based on the hillshade maps. All lunar craters selected for analysis can be found in Table S1 in the supporting information. The percent of craters removed from each experimental region ranged from 0.00% to 11.29%.

The statistics of our research are illustrated in Table 5. Among the selected 849 lunar fresh small craters, there are 418 located in maria regions and 431 in highland regions. The diameters of these craters range from 20.00 to 352.38 m, and their depths range

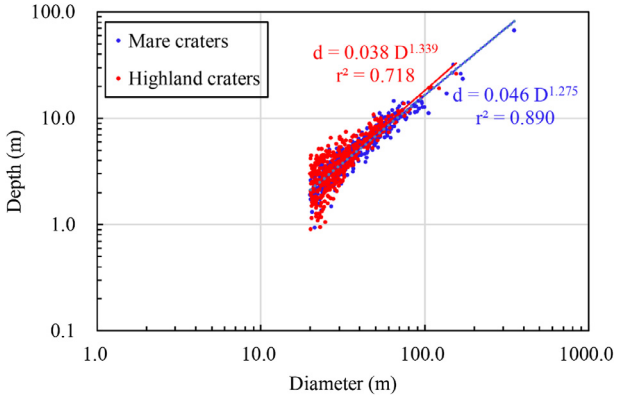

Fig. 6. Relationship of depth and diameter of lunar fresh small craters.

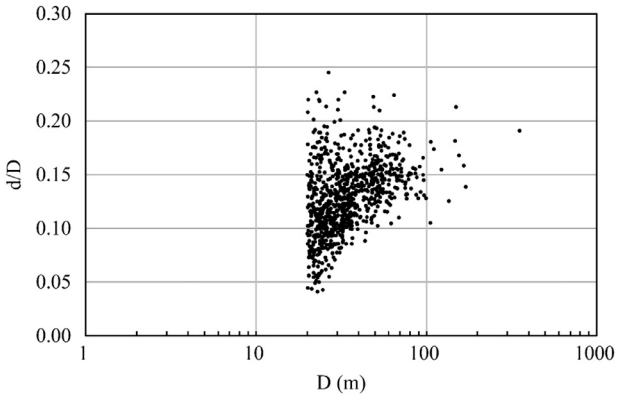

Fig. 7. Relationship between *d*/*D* ratio and diameter of lunar fresh small craters.

from 0.90 to 67.34 m. The mean *d*/*D* ratio of these craters is 0.13, i.e., shallower than 0.20. The *d*/*D* ratios of craters in the lunar mare and highland regions are approximately the same, which is in agreement with the results of Pike (1974), though this differs from what other researchers have found (e.g., Wood and Anderson, 1978; Stopar et al., 2017).

Fig. 6 shows the depth versus diameter of the selected craters in a logarithmic coordinate system, in which blue dots represent mare craters and red dots represent highland craters. It can be seen that the data for highland craters and mare craters generally overlap. Yet power law fitting results indicate a small difference between highland craters and mare craters. In addition, Fig. 6 also shows that both highland craters and mare crater depths appear more scattered at smaller diameters.

Fig. 7 shows the relationship between the *d*/*D* ratio and diameter of lunar fresh small craters, and Fig. 8 shows a histogram of the

Table 4
Number of lunar fresh small craters before and after filtering based on hillshade maps.

Region	Center Coordinates (N, E)	No. of craters before filtering	No. of craters after filtering	Percent of removed craters (%)
Mare 1	(0.65, 23.51)	50	47	6.00
Mare 2	(−3.04, −23.42)	32	30	6.25
Mare 3	(−3.66, −17.48)	62	62	0.00
Mare 4	(26.08, 3.65)	43	41	4.65
Mare 5	(20.17, 30.77)	150	150	0.00
Mare 6	(−14.66, −8.94)	91	88	3.30
Highland 1	(−43.90, 153.90)	108	99	8.33
Highland 2	(−8.99, 15.51)	28	28	0.00
Highland 3	(−41.84, 95.94)	25	24	4.00
Highland 4	(47.07, 166.93)	15	15	0.00
Highland 5	(5.92, 161.42)	120	112	6.67
Highland 6	(3.58, −100.13)	29	29	0.00
Highland 7	(47.58, −116.11)	14	14	0.00
Highland 8	(−47.95, −73.23)	124	110	11.29

Table 5
Statistics of lunar fresh small craters.

Region	Number of craters	Minimum d (m)	Maximum d (m)	Minimum D (m)	Maximum D (m)	Mean *d*/*D*	Median *d*/*D*	Standard error (m)
Mare	418	0.93	67.34	20.01	352.38	0.13	0.13	0.03
Highland	431	0.90	26.10	20.00	155.37	0.13	0.13	0.04
Total	849	0.90	67.34	20.00	352.38	0.13	0.13	0.03

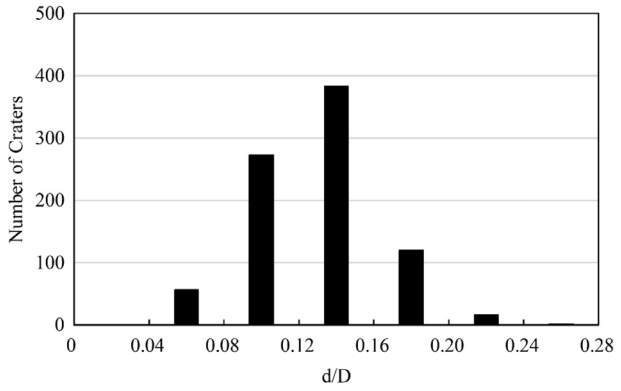

Fig. 8. Histogram of *d*/*D* ratio of lunar fresh small craters.

d/*D* ratio of lunar fresh small craters. It can be seen from Fig. 7 that the diameter of most craters in our research is < 100 m (only 11 craters > 100 m across). The *d*/*D* ratio of craters of the same diameter show large variation; however, the *d*/*D* ratio of more than 91% craters is 0.08–0.20 (Fig. 8).

5. Discussion

5.1. Comparison between mare craters and highland craters

To confidently make comparison between the most pristine mare and highland craters, we use the "deepest craters" as described in Boyce and Garbeil (2007) and Robbins and Hynek (2012). Mare and highland craters were separately divided into diameter bins and a power law was fit to the deepest craters in each bin. The diameter size of each bin was set to be 20 m ≤ D < 25 m, 25 m ≤ D < 30 m, 30 m ≤ D < 35 m, 35 m ≤ D < 40 m, 40 m ≤ D < 45 m, 45 m ≤ D < 50 m, 50 m ≤ D < 60 m, 60 m ≤ D < 70 m, 70 m ≤ D < 80 m, 80 m ≤ D < 150 m. Craters with diameter larger than 150 m were too few to be included. A power law was fit to one, two, three, four and five deepest craters in each bin of mare and highland craters. For mare craters, the power law exponent decreases with increasing numbers of craters, and tends to be a constant for more than three craters per bin with a mean 1.065 ± 0.039; the amplitude increases with increasing numbers of craters, and also reaches a constant level for more than four craters per bin with a mean 0.139 ± 0.015. For highland craters, the exponent and amplitude of power law fits show opposite variations: the power law exponent increases with increasing numbers of craters, while the amplitude decreases with increasing numbers of craters, but neither of these two parameters reaches a constant level. According to the trend of power law exponent and amplitude of highland craters, it may be conjectured that with enough samples, the power law fit of highland craters might get closer to that of mare craters. We tried to fit a power law using six deepest craters in each bin of highland craters, however, there are only eight bins left and we get $d = 0.450D^{0.755}$. Despite of that, the possibility remains to be verified with more data samples.

Using the five deepest craters in each bin, we derive

$$d = (0.471 \pm 0.080)D^{0.762\pm0.038} \quad (n = 50\,\text{highland craters}) \qquad (1)$$

$$d = (0.139 \pm 0.015)D^{1.065\pm0.039} \quad (n = 50\,\text{mare craters}). \qquad (2)$$

Judging from the power law fits of mare and highland craters, it seems that mare and highland craters are subject to different laws and highland craters tend to have more scatter than mare craters. Wood and Anderson (1978) also reported different power laws for mare craters ($d = 0.170D^{1.070}$) and highland craters ($d = 0.181D^{0.969}$) with diameters 0.50–20 km. It is notable that the power law of mare craters of Wood and Anderson (1978) and our research agree well, while that of highland craters differ greatly from each other. Terrain-related differences might account for the difference. According to Melosh (1989), lunar craters smaller than "200–400 m" in diameter are in the strength-dominated regime. The craters in our research are all within this regime, and their morphologies may be strongly influenced by the cohesive strength of the target material. It is well known that the surficial layer of the Moon is covered by lunar regolith with thickness varying from place to place, and the average thickness of lunar regolith is about 4–5 m for maria and 10–15 m for highlands (e.g., McKay et al., 1991; Shkuratov and Bondarenko, 2001; Fa and Jin, 2010). As a result, fresh craters with diameters less than tens of meters were probably formed in this layer.

The Lunar Penetrating Radar (LPR) onboard the Chang' E-3 mission identified more than nine subsurface layers along the rover path, even within the first upper ten meters the lunar regolith could be divided into at least three layers, suggesting that the region has experienced complex geological processes (Xiao et al., 2015; Zhao et al., 2014). The physical properties of materials in different subsurface layers such as density and porosity can be

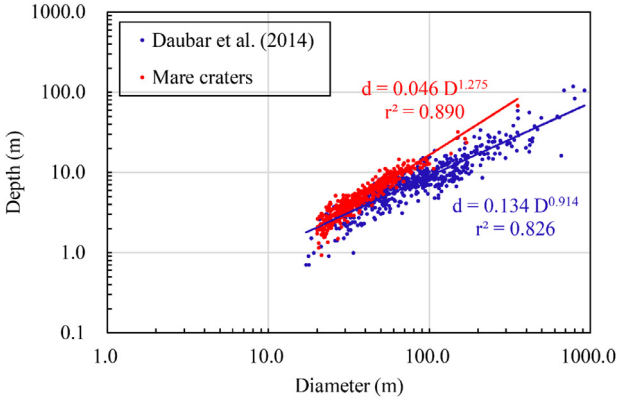

Fig. 9. Comparison of our statistics and those of Daubar et al. (2014).

very different, which may affect the morphology of craters formed within these layers. Various properties of the lunar regolith might lead to the scatter in depths for craters with similar diameters (Figs. 6 and 7), as well as the difference between highland and mare craters.

5.2. Comparison with other small lunar crater statistics

Daubar et al. (2014) produced d/D ratio statistics for the Apollo 15 landing site and Mare Ingenii using LRO NAC DEM data. The diameters of craters they sampled vary from 17.01 m to 918.56 m, and their depths vary from 0.70 m to 117.6 m. Fig. 9 shows the comparison of our results and those of Daubar et al. (2014). At small diameters the two results seem consistent, but craters in our results tend to be deeper than that in Daubar et al. (2014) as diameter increases. The power law relationship in Daubar et al. (2014) also reflects a shallower slope than our data.

Comparison between the deepest lunar mare craters of Daubar et al. (2014) and mare craters in our research was also conducted. The lunar craters in Daubar et al. (2014) were divided into diameter bins as described in 5.1, generating 11 bins altogether, including craters more than 150 m diameter. A power law was fit to one, two, three, four and five deepest craters in each bin and we get

$$d = (0.140 \pm 0.007)D^{1.007\pm0.013} \quad (n = 55). \tag{3}$$

Amazingly, the power law amplitudes of mare craters in Eqs. (2) and (3) almost coincide, and the power law exponent of the two equations are also consistent within two standard deviations. Therefore, from the perspective of power law fit (using the deepest craters), results of our research and that of Daubar et al. (2014) agree well.

The average d/D ratio of craters of Daubar et al. (2014) was 0.096, shallower than 0.2. Both the mean and median d/D ratio in our research are 0.13 ± 0.03, which is approximate to that of Daubar et al. (2014) and consistent with that of Mahanti et al. (2012, 2014) and Stopar et al. (2017). From this perspective, our results are generally in agreement with recent studies.

5.3. Effects of different methods

The shadow measurement technique has been widely used to determine crater depths on many solar system bodies (e.g., Arthur, 1974; Pike, 1980; Schenk, 1989) because it is simple and requires only one image at lower sun angles. The original shadow measurement technique only applies to craters with shadow lengths $\sim D/2$. Chappelow and Sharpton (2002) presented a more precise and general method by assuming simple crater shapes to be paraboloid, cone or flat-floored. For each kind of crater he gave an equation for determining crater depth in terms of shadow length and solar incidence angle. This method has been demonstrated to give reliable depths for craters with diameters larger than 10 times the pixel scale (Herrick, 2013).

Comparison of the measurement techniques from the shadow and DEM using the same dataset showed that the average of the absolute value of the differences in d/D could be 15% (Daubar et al., 2014). In addition, some craters might be irregular and they cannot be cataloged into paraboloid, cone or flat-floored shaped, which can also introduce errors. Therefore, direct measurement from stereo products is a better method to determine crater morphologic parameters, and shadow measurement technique could be a supplementary method when stereo products are not available. Chappelow (2013, 2017) have considerably extended this shadow method to fit any conic section shaped crater, however, since most early studies about crater depth and diameter were carried out using the earliest shadow measurement technique, the difference between our results and those derived from this shadow measurement technique may be partly attributed to the effects of different methods.

6. Conclusions

In this research, we conducted a comprehensive study of the depth and diameter relationship of subkilometer-diameter craters on the lunar surface using high-resolution images and related mapping products. The fresh small craters examined were selected from lunar maria and highland regions based on features indicating that they are relatively fresh and unmodified, and filtered further based on hillshade maps to ensure reliability. The statistics showed the d/D ratios of the sampled craters were about 0.13, in accordance with similar research and shallower than similarly well-preserved craters with diameter > 1 km. The shallower ratio is probably caused by the strength properties of the surface and shallow subsurface, or the different methods used. The fitted power law parameters of highland and mare craters were found to be different, which may be explained by terrain-related differences. In future, the detailed mechanism of the creation of small craters should be studied using numerical simulations and/or physical experiments.

Acknowledgments

This work was supported by the National Natural Science Foundation of China (Grant Nos. 41490635, 41590851, and 41472303) and the Strategic Priority Research Program of the Chinese Academy of Sciences with the project “Digital Moon and Earth-Moon System Evolution”. We are grateful to reviewer Stuart Robbins and Chappelow J. E. for their insightful comments and constructive suggestions on this paper. The authors gratefully acknowledge the LROC team for providing the data products used in this research. The authors also thank Thomas Kneissl for providing the *CraterTools* software. Finally, the authors would like to thank Editage [www.editage.cn] for English language editing.

Supplementary materials

Supplementary material associated with this article can be found, in the online version, at doi:10.1016/j.icarus.2018.02.031.

References

Albee, A.L., Palluconi, F.D., Arvidson, R.E., 1998. Mars global surveyor mission: overview and status. Science 279 (5357), 1671–1672. doi:10.1126/science.279.5357.1671.

Arthur, D.W.G., 1974. Lunar crater depths from Orbiter IV long-focus photographs. Icarus 23 (1), 116–133. https://doi.org/10.1016/0019-1035(74)90109-2.

Baldwin, R.B., 1963. The Measure of the Moon. University of Chicago Press, Chicago.

Baldwin, R.B., 1965. The crater diameter–depth relationship from Ranger VII photographs. Astron. J. 70 (8), 545–547. doi:10.1086/109778.

Barnouin, O.S., Zuber, M.T., Smith, D.E., Neumann, G.A., Herrick, R.R., Chappelow, J.E., Murchie, S.L., Prockter, L.M., 2012. The morphology of craters on Mercury: results from MESSENGER flybys. Icarus 219 (1), 414–427. http://doi.org/10.1016/j.icarus.2012.02.029.

Bouška, J., 1968. Crater diameter-depth relationship from ranger lunar charts. Bull. Astron. Inst. Czechoslov. 19, 229.

Boyce, J.M., Garbeil, H., 2007. Geometric relationships of pristine Martian complex impact craters, and their implications to Mars geologic history. Geophys. Res. Lett. 34, L16201. doi:10.1029/2007GL029731.

Chappelow, J.E., Sharpton, V.L., 2002. An improved shadow measurement technique for constraining the morphometry of simple impact craters. Meteorit. Planet. Sci. 37 (4), 479–486. doi:10.1111/j.1945-5100.2002.tb00834.x.

Chappelow, J.E., 2013. Simple impact crater shape determination from shadows. Meteorit. Planet. Sci. 48 (10), 1863–1872. doi:10.1111/maps.12201.

Chappelow, J.E., 2017. On the depths and shapes of the freshest kilometer-scale simple craters on the lunar maria: a new crater shape model. Meteorit. Planet. Sci. doi:10.1111/maps.12853.

Cintala, M.J., Mouginis-Mark, P.J., 1980. Martian fresh crater depths: more evidence for subsurface volatiles. Geophys. Res. Lett. 7, 329–332. doi:10.1029/GL007i005p00329.

Daubar, I.J., Atwood-Stone, C., Byrne, S., McEwen, A.S., Russell, P.S., 2014. The morphology of small fresh craters on Mars and the Moon. J. Geophys. Res.: Planets 119 (12), 2620–2639. doi:10.1002/2014JE004671.

Fa, W., Jin, Y., 2010. A primary analysis of microwave brightness temperature of lunar surface from Chang-E 1 multi-channel radiometer observation and inversion of regolith layer thickness. Icarus 207 (2), 605–615. http://dx.doi.org/10.1016/j.icarus.2009.11.034.

Herrick, R.R., 2013. The shapes of simple craters in the outer solar system determined with an enhanced shadow measurement technique. In: Lunar Planetary Science Conference, 44, p. 2825.

Jaumann, R., Neukum, G., Behnke, T., Duxbury, T.C., Eichentopf, K., Flohrer, J., Gasselt, S.v., Giese, B., Gwinner, E., Hauber, E., Hoffmann, H., Hoffmeister, A., Köhler, U., Matz, K.–D., McCord, T.B., Mertens, V., Oberst, J., Pischel, R., Reiss, D., Ress, E., Roatsch, T., Saiger, P., Scholten, F., Schwarz, G., Stephan, K., Wählisch, M.the HRSC Co-Investigator Team, 2007. The high-resolution stereo camera (HRSC) experiment on Mars express: instrument aspects and experiment conduct from interplanetary cruise through the nominal mission. Planet. Space Sci. 55 (7-8), 928–952. https://doi.org/10.1016/j.pss.2006.12.003.

Kato, M., Sasaki, S., Takizawa, Y., 2010. The Kaguya mission overview. Space Sci. Rev. 154 (1-4), 3–19. doi:10.1007/s11214-010-9678-3.

Kneissl, T., van Gasselt, S., Neukum, G., 2011. Map-projection-independent crater size–frequency determination in GIS environments - New software tool for ArcGIS. Planet. Space Sci. 59 (11), 1243–1254. http://doi.org/10.1016/j.pss.2010.03.015.

Mahanti, P., Robinson, M.S., Stelling, R., 2012. Depth-to-diameter ratio and slopes in small lunar highland craters. AGU Fall Meeting Abstracts.

Mahanti, P., Robinson, M.S., Stelling, R., 2014. How deep and steep are small lunar craters?—New insights from LROC NAC DEMs. In: Lunar and Planetary Science Conference, 45, p. 1584.

Malin, M.C., Dzurisin, D., 1977. Landform degradation on Mercury, the Moon, and Mars: evidence from crater depth/diameter relationships. J. Geophys. Res. 82 (2), 376–388. doi:10.1029/JB082i002p00376.

Markov, A.V., 1967. On the relative depths of the Moon's mountain rings and craters in the region of Mare Nubium. Proc. R. Soc. Lond. Ser. A, Math. Phys. Sci. 296 (1446), 432–434. doi:10.1098/rspa.1967.0035.

McKay, D.S., Heiken, G., Basu, A., Blanford, G., Simon, S., Reedy, R., French, B.M., Papike, J., 1991. The lunar regolith. Lunar Sourcebook: A User's Guide to the Moon 285–356 Archive.

Melosh, H.J., 1989. Impact Cratering: A Geologic Process. Oxford University Press, New York, p. 253.

Mouginis-Mark, P.J., Boyce, J., Sharpton, V.L., Garbeil, H., 2017. Determination of Mars crater geometric data: insights from high-resolution digital elevation models. Meteorit. Planet. Sci. doi:10.1111/maps.12895.

Pike, R.J., 1974. Depth/diameter relations of fresh lunar craters: revision from spacecraft data. Geophys. Res. Lett. 1 (7), 291–294. doi:10.1029/GL001i007p00291.

Pike, R.J., 1977. Apparent depth/apparent diameter relation for lunar craters. In: Lunar and Planetary Science Conference Proceedings, 8, pp. 3427–3436.

Pike, R.J., 1980. Control of crater morphology by gravity and target type-Mars, Earth, Moon. In: Lunar and Planetary Science Conference Proceedings, 11, pp. 2159–2189.

Robbins, S.J., Antonenko, I., Kirchoff, M.R., Chapman, C.R., Fassett, C.I., Herrick, R.R., Singer, K., Zanetti, M., Lehan, C., Huang, D., Gay, P.L., 2014. The variability of crater identification among expert and community crater analysts. Icarus 234, 109–131. doi:10.1016/j.icarus.2014.02.022.

Robbins, S.J., Hynek, B.M., 2012. A new global database of Mars impact craters ≥1 km: 2. Global crater properties and regional variations of the simple-to-complex transition diameter. J. Geophys. Res. 117, E06001. doi:10.1029/2011JE003967.

Robinson, M.S., Brylow, S.M., Tschimmel, M., Humm, D., Lawrence, S.J., Thomas, P.C., Denevi, B.W., Bowman-Cisneros, E., Zerr, J., Ravine, M.A., Caplinger, M.A., Ghaemi, F.T., Schaffner, J.A., Malin, M.C., Mahanti, P., Bartels, A., Anderson, J., Tran, T.N., Eliason, E.M., McEwen, A.S., Turtle, E., Jolliff, B.L., Hiesinger, H., 2010. Lunar reconnaissance orbiter camera (LROC) instrument overview. Space Sci. Rev. 150 (1-4), 81–124. doi:10.1007/s11214-010-9634-2.

Salamunićcar, G., Lončarić, S., Mazarico, E., 2012. LU60645GT and MA132843GT catalogues of Lunar and Martian impact craters developed using a Crater Shape-based interpolation crater detection algorithm for topography data. Planet. Space Sci. 60 (1), 236–247. doi:10.1016/j.pss.2011.09.003.

Schenk, P.M., 1989. Crater formation and modification on the icy satellites of Uranus and Saturn: depth/diameter and central peak occurrence. J. Geophys. Res.: Solid Earth 94 (B4), 3813–3832. doi:10.1029/JB094iB04p03813.

Shkuratov, Y.G., Bondarenko, N.V., 2001. Regolith layer thickness mapping of the Moon by radar and optical data. Icarus 40 (2), 329–338. http://dx.doi.org/10.1006/icar.2000.6545.

Stopar, J.D., Robinson, M.S., Barnouin, O., McEwen, A., Speyerer, E.J., Henriksen, M.R., Sutton, S.S., 2017. Relative depths of simple craters and the nature of the lunar Regolith. Icarus 298, 34–48. https://doi.org/10.1016/j.icarus.2017.05.022.

Vondrak, R., Keller, J., Chin, G., Garvin, J., 2010. Lunar reconnaissance orbiter (LRO): observations for lunar exploration and science. Space Sci. Rev. 150 (1-4), 7–22. doi:10.1007/s11214-010-9631-5.

Watters, W.A., Geiger, L.M., Fendrock, M., Gibson, R., 2015. Morphometry of small recent impact craters on Mars: size and terrain dependence, short-term modification. J. Geophys. Res.: Planets 120 (2), 226–254. doi:10.1002/2014JE004630.

Wood, C.A., Anderson, L., 1978. New morphometric data for fresh lunar craters. In: Lunar and Planetary Science Conference Proceedings, 9, pp. 3669–3689.

Xiao, L., Zhu, P., Fang, G., Xiao, Z., Zou, Y., Zhao, J., Zhao, N., Yuan, Y., Qiao, L., Zhang, X., Zhang, H., Wang, J., Huang, J., Huang, Q., He, Q., Zhou, B., Ji, Y., Zhang, Q., Shen, S., Li, Y., Gao, Y., 2015. A young multilayered terrane of the northern Mare Imbrium revealed by Chang'E-3 mission. Science 347 (6227), 1226–1229. http://dx.doi.org/10.1126/science.1259866.

Zhao, B., Yang, J., Wen, D., Gao, W., Chang, L., Song, Z., Xue, B., Zhao, W., 2011. Overall scheme and on-orbit images of Chang'E-2 lunar satellite CCD stereo camera. Sci. China Technol. Sci. 54, 2237–2242. doi:10.1007/s11431-011-4519-5.

Zhao, N., Zhu, P., Yang, K., Yuan, Y., Guo, S., 2014. The preliminary processing and analysis of LPR channel-2B data from Chang'E-3. Sci. China Phys., Mech. Astron. 57 (12), 2346–2353. http://dx.doi.org/10.1007/s11433-014-5590-2.

Zurek, R.W., Smrekar, S.E., 2007. An overview of the Mars reconnaissance orbiter (MRO) science mission. J. Geophys. Res.: Planets 112 (E5). doi:10.1029/2006JE002701.